

ChemComm

Chemical Communications

Accepted Manuscript

This article can be cited before page numbers have been issued, to do this please use: A. Kuzume and S. Kume, *Chem. Commun.*, 2024, DOI: 10.1039/D4CC03973D.



This is an Accepted Manuscript, which has been through the Royal Society of Chemistry peer review process and has been accepted for publication.

Accepted Manuscripts are published online shortly after acceptance, before technical editing, formatting and proof reading. Using this free service, authors can make their results available to the community, in citable form, before we publish the edited article. We will replace this Accepted Manuscript with the edited and formatted Advance Article as soon as it is available.

You can find more information about Accepted Manuscripts in the [Information for Authors](#).

Please note that technical editing may introduce minor changes to the text and/or graphics, which may alter content. The journal's standard [Terms & Conditions](#) and the [Ethical guidelines](#) still apply. In no event shall the Royal Society of Chemistry be held responsible for any errors or omissions in this Accepted Manuscript or any consequences arising from the use of any information it contains.

ARTICLE

Spectrometric Monitoring of CO₂ Electrolysis on a Molecularly Modified Copper Surface

Akiyoshi Kuzume^{*a} and Shoko Kume^{*b}Received 00th January 20xx,
Accepted 00th January 20xx

DOI: 10.1039/x0xx00000x

Since copper has been extensively studied due to its unique ability to reduce carbon dioxide to hydrocarbons and alcohols, it tends to yield a mixture of products. Among various efforts to improve the selectivity and efficiency of this catalysis, the introduction of organic molecules and polymers on the copper/electrolyte interface has proven to be an effective and promising way to improve surface activity, considering the variation and precise designability of organic structure. The role of surface molecular modifiers, however, is not as simple as that in homogeneous catalysts, and understandings of a wide scale of interactions from atomic scale to whole electrode structure is required. This feature article classifies those different scale interactions caused by organic modifiers on copper catalysts, together with the experimental support by *in situ* vibrational spectroscopy which directly observes surface species and events. Based on these recent understandings, novel fabrication methods of organic structure on copper catalysts is also discussed.

1. Introduction

Carbon neutralization is an effort to achieve net-zero carbon dioxide (CO₂) production by balancing the emission and absorption of carbon to and from the atmosphere. Because 90% of the total emitted greenhouse gases has been generated by the combustion of fossil fuels, considerable research has been conducted to decrease, fix, and recycle CO₂ to realize carbon neutralization. Since it is unrealistic to lower CO₂ emissions to zero, so much attention has been paid to developing technology to increase CO₂ removal from the atmosphere through capture and storage. Electrochemical and chemical conversion technologies that can effectively convert CO₂ to (bio)fuels, syngas, synthetic materials, and plastics are attracting interest from the perspective of sustainable development goals and carbon neutralization, not only for CO₂ fixation but also to generate alternative fuels to petroleum. Electrochemical reduction of CO₂, that has been studied since the 19th century¹, progresses via a multi-step reaction involving multiple electrons and protons (H⁺) and generates various chemicals such as carbon monoxide (CO), formate, hydrocarbons, and alcohol depending on the electrode material and solvent used². The CO₂ reduction reaction (CO₂RR) is accompanied by the hydrogen evolution reaction (HER) as a parasitic side reaction, which complicates the elucidation of the mechanism of the CO₂RR. In the 1990s, Hori et al.³ roughly classified metal electrodes into

four types according to the reaction selectivity and main products, i) metals that mainly produces CO due to weak CO adsorption (Au, Ag, and Zr), ii) metals that mainly produce formate (Pb, Hg, Cd, Tl, In, and Sn), iii) metals that suppress CO₂RR due to CO poisoning (Pt, Ni, Fe, and Ti), which results in the dominant formation of hydrogen gas, and iv) Cu, that can produce hydrocarbons such as methane, ethylene, and alcohol. The unique activity of Cu is caused by moderate stabilization of adsorbed CO, allowing it to be further reduced to various hydrocarbons. As a result, optimizing the Cu catalyst for CO₂RR to capture and effectively convert CO₂ to useful materials has been extensively investigated for the last three decades.

Since the first report of Cu CO₂RR producing hydrocarbons by Hori et al.^{4,5}, new aspects of this reaction have been discovered with development of new catalysts. In 2011, Kanan et al.⁶ prepared a Cu catalyst by reducing copper oxide which exhibited CO₂ reduction with much lower overpotential. Subsequent studies showed that Cu catalysts derived from oxides and hydroxides were effective for C₂₊ production^{7,8}. The favorable performance of Cu in the CO₂RR has been ascribed to many factors such as i) adsorbed CO activity is affected by the remaining oxides and Cu⁺ species during the CO₂RR⁹⁻¹¹, ii) formation of active Cu atoms at grain boundaries¹²⁻¹³, and iii) faceting of the Cu surface¹⁴. Bell et al.¹⁵ observed that the CO₂RR was strongly dependent on the alkali metal cations present in the electrolyte, which revealed the importance of water molecules at the electrode surface acting as an H⁺ source in the

^a Clean Energy Research Center, Yamanashi University, Kofu, 400-8510, Japan. E-mail: akuzume@yamanashi.ac.jp

^b Graduate School of Advanced Science and Engineering, Hiroshima University, Higashi-Hiroshima, 739-8526, Japan. E-mail: skume@hiroshima-u.ac.jp



CO₂RR. Roldan Cuenya and co-workers showed that their Cu cube catalyst exhibited dynamic structural changes during the CO₂RR even when Cu was zero-valent¹⁶. The generation of C₂₊ products requires C-C bond formation on the catalyst surface, so it is also affected by the partial pressure of CO₂¹⁷.

These discoveries on the CO₂RR activity of nanostructured Cu surfaces have revealed the unique features of this electroreduction process. First, CO₂ is hardly soluble in water and its supply to the electrode surface is as important as the catalyst surface activity in determining CO₂RR activity. Second, CO₂ reduction consumes H⁺ and produces hydroxide anions (OH⁻). Therefore, the behavior of water, the most common H⁺ supplier, can determine catalytic efficiency. Third, the way H⁺ is supplied to the electrode surface and local pH affect CO₂ reduction and determine the favored product. Fourth, the Cu surface is not robust during electroreduction; its structure often evolves to a more stable configuration under the applied cathodic potential and is affected by other chemical conditions. These interfacial insights notified researchers to carefully evaluate CO₂RR performance¹⁸.

Along with the catalyst development, molecular processes of CO₂RR on Cu have been extensively discussed. They involve branching of the intermediates because Cu normally forms multiple carbonaceous products, even from a single crystal facet. These complex hydrocarbon-generation mechanisms and reaction pathways have been reviewed by Koper and colleagues (Figure 1)¹⁹. Numerous experimental and theoretical studies have been conducted to elucidate the reaction mechanism and pathways of the electrochemical CO₂RR and mechanistic insights for the design of efficient and selective Cu-based catalysts for the CO₂RR have been outlined in multiple reviews²⁰⁻²⁵.

With these progress in Cu electrocatalyst, organic modification of Cu targeting CO₂RR promotion have also been focused. In 2016, Wang's group reported the earliest attempt to modify the Cu catalyst surface with organic moieties to improve CO₂RR activity by using various amino acids as modifiers²⁶. This and other early studies²⁷⁻²⁹ mainly focused on the local molecular interactions of CO₂ and/or its reduction intermediates on Cu surfaces with introduced chemical moieties. In 2019, Toste et al.³⁰ demonstrated the universal effect of various polymers and molecules on the Cu CO₂RR, revealing that organic species affect catalysis by regulating the behavior of water on the Cu catalyst surface. In 2021, Goddard and co-workers showed that the components of a polymer modifier included in the catalytic system cooperatively improved the C₂₊ production selectivity³¹. They suggested that the modifier is likely to induce a combination of nonspecific effects such as increased local CO₂ concentration, increased porosity for gas diffusion, and a local electric field effect rather than the specific molecular interactions of the components affecting CO₂RR activity.

Considering these findings, it came to be recognized that the effect of organic modifiers on CO₂RR activity needs to be studied from a wider perspective, spanning the specific interactions between Cu atoms and reaction intermediates; the CO₂ and H⁺ supply path to the active electrode surface; and larger-scale catalyst assemblies that involve three-phase

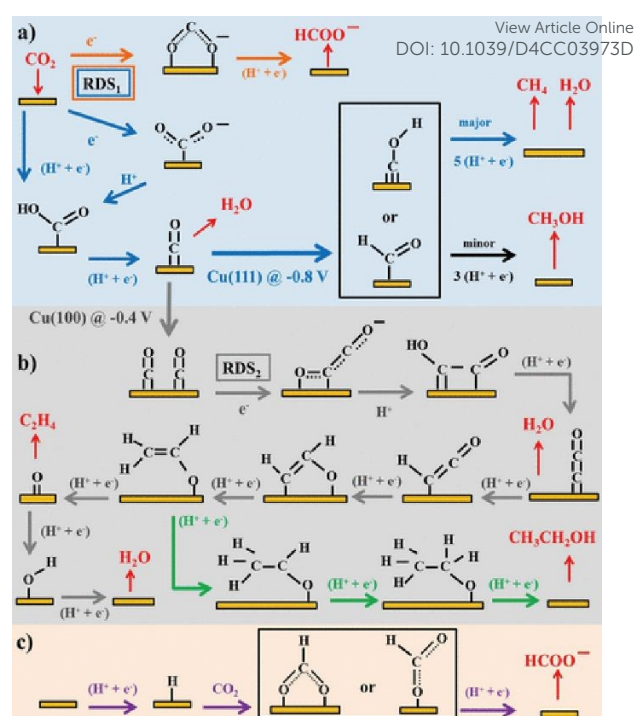


Figure 1. Schemes of possible reaction pathways of the CO₂RR on transition metals. (a) pathway from CO₂ to CO, CH₄, CH₃OH, and formate, (b) pathways from CO₂ to ethylene and ethanol, and (c) pathway of CO₂ insertion into a metal-H bond yielding formate. Adapted with permission from ref 19. Copyright 2015 American Chemical Society.

interfaces (CO₂ gas/liquid electrolyte/solid Cu)^{32,33}. To evaluate this wide range of factors, direct observation of the catalyst surface during operation is essential. *In situ* observation with Raman and infrared (IR) spectroscopy is a powerful tool to elucidate the species present and events occurring on working catalyst surfaces. Vibrational spectroscopic techniques enable us to evaluate the reaction intermediate structure, the ratio of species involved in H⁺ transfer, and the state of the Cu surface. This direct information can help us to elucidate the role of organic modifiers in improving CO₂RR activity.

In this feature article, we first introduce the use of vibrational spectroscopy to investigate the CO₂RR process on catalyst surfaces. Next, recent research on organic modification of Cu catalysts to increase CO₂RR efficiency is presented. The studies are classified according to the role of the organic modifier, which is determined based on the *in situ* observation of the active catalyst surface. Finally, we introduce recent research on the development of organic modifiers to maximize their potential functions. Here we only cover studies that use vibrational spectroscopy; other reviews of Cu electrocatalysis and the role of organic modifiers in the CO₂RR can be found elsewhere^{34,35}.



2. Application of vibrational spectroscopy to the CO₂RR on copper electrocatalysts

2.1 Vibrational spectroscopy for *in situ* interfacial analysis of electrocatalysis

Electrochemical reduction reactions of CO₂ that occur on electrode surfaces involve multi-electron and multi-proton transfers, making *in situ* interfacial analysis invaluable for evaluating and understanding reaction activity and mechanisms to characterize innovative high-performance catalysts. In particular, vibrational spectroscopic techniques such as Raman spectroscopy and IR absorption spectroscopy can provide chemical information about adsorbates, water molecules, and reaction intermediates during electrochemical reactions under applied potential, thus allowing elucidation of electron transfer and chemical reaction processes at solid-liquid interfaces. Vibrational spectroscopy is also sensitive to local interfacial pH and electrode oxidation state, making it a powerful analytical method to evaluate complex surface processes of the CO₂RR.

Raman scattering light³⁶ contains information about the molecular vibrations of the material, but its scattering cross section (intensity) is much weaker than that of elastically scattered light (Rayleigh scattering). Surface-enhanced Raman spectroscopy (SERS) is a powerful tool to detect surface species with high sensitivity³⁷⁻³⁹. Surface plasmon resonance (SPR), which typically occurs on rough and nanostructured surfaces of coinage metals (Au, Ag, and Cu), is the surface-localized resonance between incident light and the collective oscillations of the conduction electrons on a metal surface, inducing local electromagnetic fields that enhances Raman signals. Chemical enhancement effect, on the other hand, originates from electronic interactions, including charge transfer between the metal surface and adsorbed molecules; this effect is selective for the first layer of adsorbed species on a metal surface. These two enhancement effects allow SERS to be used as a surface-selective, non-destructive, and highly sensitive analytical method for solid surfaces.

Surface-enhanced infrared absorption spectroscopy (SEIRAS) is another type of vibrational spectroscopy that can detect adsorbed species with high selectivity and sensitivity^{40,41}. Adequate surface enhancement requires a nanostructured thin film of coinage metal adhered to the surface of an IR-transparent prism. The plasmonic fields generated on the coinage metal surface strongly contribute to the enhancement mechanism, selectively enhancing molecular signals in the immediate vicinity of the surface. In addition, SEIRAS in an attenuated total reflection (ATR) configuration allows for unrestricted mass transport to/from the electrode surface, making it suitable for investigating gas-evolving reactions such as the CO₂RR.

SEIRAS detects vibrational modes of molecules with large dipole moments, whereas Raman spectroscopy detects vibrational modes with high symmetry that have a large change in polarizability. Therefore, the combined use of SEIRAS and Raman spectroscopy in a complementary manner can provide comprehensive chemical information about a metal catalyst surface, such as molecular structure, crystal structure,

adsorption geometry, and adsorbate configuration, extracting mechanistic information and establishing structure-activity relationships. Both IR and Raman spectroscopies can be used for *in situ* observation of solid-liquid interfaces and therefore are widely utilized in the study of electrochemical CO₂ reduction. It is important to point out that SEIRAS and SERS are frequently employed in the assumption that they provide largely overlapping information regarding reaction intermediates. To confirm this, Chang and co-workers investigated CO adsorption on Pt, Pd, Au, and Cu using both surface-enhanced spectroscopic techniques⁴². SEIRAS and SERS provided similar spectral information in terms of peak position and Stark tuning rate on strongly adsorbing surfaces (Pd and Pt), but probed different subpopulations of adsorbates on weakly adsorbing surfaces (Au and Cu) because of competitive adsorption of water molecules. Complementary density functional theory (DFT) calculations confirmed the lack of scaling between the derivatives of the dipole moment and polarizability, indicating that the peak intensities in SEIRAS and SERS spectra do not necessarily correlate with each other.

2.2 *In situ* observation of the electrochemical CO₂RR on copper

Soon after the discovery of the SERS effect, Fleischmann's group performed *in situ* Raman spectroscopy measurements of the CO₂RR, detecting surface-adsorbed CO₂⁻ and carboxyl groups on an electrochemically roughened Ag electrode⁴³. Since then, the detection of electrochemically generated species, especially adsorbed CO on metal surfaces, by SERS has provided valuable information for elucidating the mechanism of electrochemical CO₂ reduction.

As mentioned above, Cu is the only metal that mainly produces hydrocarbon and alcohol species from the electrochemical reduction of CO₂. Using a Cu catalyst produces a wider range of intermediates than those obtained using other metals, which only produce CO or formate. It is known from the slope of the Tafel plot of the CO₂RR that the rate-determining step is the first one-electron reduction process (CO₂ + e⁻ → CO₂⁻). Considering the findings of *in situ* Raman spectroscopy and DFT calculations, Chernyshova et al.⁴⁴ reported that the intermediate formed in the first step of the CO₂RR is the carboxyl group η²(C,O)-CO₂⁻ adsorbed on the Cu surface with C and O (Figure 2). The carboxyl group was further reduced to HCOO⁻ and CO adsorbates depending on the presence of surface structures, such as defects and steps, and partial oxidation states of Cu. These intermediate adsorbates were finally converted to hydrocarbons, alcohols, and/or formate as final products of the CO₂RR.

Using a complementary combination of *in situ* Raman spectroscopy and IR spectroscopy, Ito and colleagues studies the spectral features of adsorbed species (C-O) and metal-adsorbed species (Cu-CO) on the Cu electrode surface during the CO₂RR⁴⁵. At the onset of the CO₂RR, the CO stretching vibration was observed around 2000 cm⁻¹ on the Cu surface and the Cu-CO stretching vibration was observed around 360 cm⁻¹. The intensities of both signals gradually decreased during a cathodic potential sweep accompanied by the decrease of adsorbed carbonate (CO₃²⁻). It is interesting to note that two



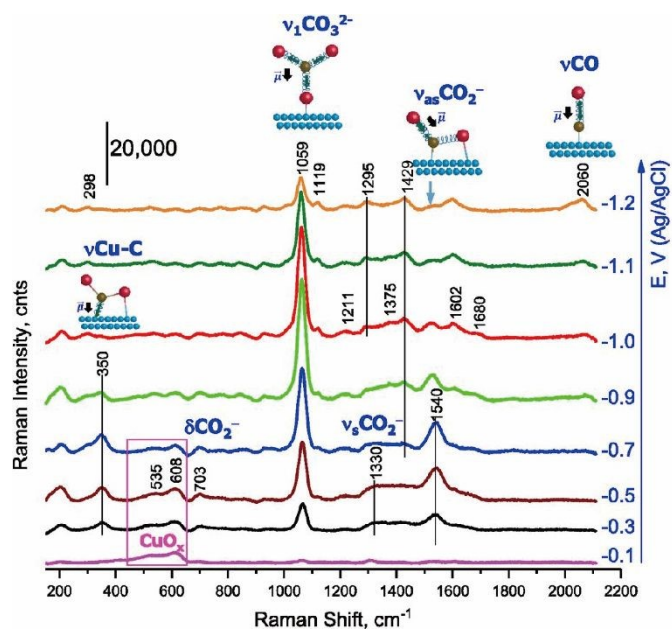


Figure 2. Operando SERS of rough Cu surface in CO_2 -saturated $0.1 \text{ dm}^{-3} \text{ NaHCO}_3$ (pH 6.8). Spectra were measured in the cathodic direction from -0.1 V . Adapted with permission from ref 44. Copyright 2018 National Academy of Sciences.

signals assigned to CO adsorbed on terrace (around 2000 cm^{-1}) and adatom defect Cu atoms (around 2100 cm^{-1})⁴⁶ were observed when CO gas was introduced onto the Cu surface, while only former appeared in *in situ* CO_2RR condition, demonstrating the ability of vibrational spectroscopy to monitor the effect of the surface structure of the Cu electrode on the CO_2RR .

In situ Raman and IR spectroscopies are capable of not only detecting adsorbate species, but also monitoring the oxidation state of Cu, the role of interfacial water, and the effect of surface reconstruction, providing information that can be used to improve CO_2RR efficiency and selectivity. Mandal et al. performed *in situ* Raman spectroscopy focusing on adsorbed CO and the oxidation state of the Cu surface during the CO_2RR on various Cu_2O nanostructures to clarify the effect of the CO adsorption affinity on the reaction efficiency and selectivity⁴⁷. The Cu_2O surface was immediately reduced at the potential onset of the CO_2RR and CO was adsorbed in an on-top configuration on the exposed metallic Cu sites. The selective formation of C_{2+} products proceeded only after the reduction of Cu_2O to metallic Cu. In addition, the Raman signal intensity of adsorbed CO related to the proportion of under-coordinated sites such as defects and boundaries on the metal surface. The increased population of adsorbed CO is likely to result in multi-carbon products.

The correlation between the potential-dependent CO coverage and selective production of C_{2+} was also demonstrated in a study of the CO_2RR with Cu_2O nanocubes using operando Raman spectroscopy⁴⁸. Zhan and co-workers suggested that the potential-dependent intensity ratio of the Cu–CO stretching band (around 350 cm^{-1}) to the CO rotation band (around 280 cm^{-1}) followed a volcano trend, similar to the Faraday efficiency

of multi-carbon products (Figure 3). This finding illustrated that there is a clear correlation between the CO coverage of catalyst surfaces and C–C coupling modes observed in vibrational spectra.

It is important to understand the roles of the oxidation state of the Cu surface and adsorbed intermediates in the electrochemical CO_2RR . Chou et al.⁴⁹ investigated the CO_2RR mechanism with Cu catalysts in various oxidation states using *in situ* SEIRAS and X-ray absorption spectroscopy (Figure 4). They showed that CO formed at the on-top position on the electrodeposited Cu surface, which primarily has the oxidation state of Cu(I), and a C_1 hydrocarbon product was obtained during further reduction. The as-prepared Cu electrode exhibited an oxidation state of Cu(0), which promoted the generation of bridged CO, inhibiting the formation of a hydrocarbon product. In contrast, the Cu electrode seasoned by cyclic voltammetry contained both Cu(I) and Cu(0), where on-top CO and bridged CO, respectively, were observed during the CO_2RR , enhancing selective C_2 production. Therefore, the oxidation state of the Cu catalyst affected the electrocatalytic properties of the substrate–catalyst interface and modulated the CO_2 reduction mechanism.

In the CO_2RR , the presence of interfacial water directly affects the kinetics of hydrogenation steps along with the competing HER. However, the structural composition and dynamic evolution of interfacial water molecules are difficult to investigate because of the interference from bulk water and the bias dependence of interfacial water layers. Wang and co-workers used *in situ* ATR SEIRAS and *in situ* Raman spectroscopy combined with molecular dynamics simulations to probe the dynamic changes of interfacial water structure on an electrified surface and explore the mechanism of HER activity and selectivity with the goal of enhancing multi-carbon product formation⁵⁰. Their results demonstrated that the hydrogen-bonding structure of interfacial water played an important role in controlling reaction selectivity in the CO_2RR .

In situ vibration spectroscopies also can be used to monitor the effect of surface morphology at the nanoscale on CO_2RR efficiency and selectivity. Gunathunge et al.⁵¹ reported the first observation of the reversible formation of nanoscale Cu clusters on an electrode surface during the CO_2RR induced by the adsorbed CO intermediate. A series of *in situ* SEIRA and SERS spectra of the on-top CO molecules were deconvoluted into two peaks: the low-frequency band (2050 cm^{-1} , LFB) and high-frequency band (HFB, 2080 cm^{-1}) each was assigned to the CO molecules adsorbed at terrace and defect sites, respectively. The potential-dependent spectra showed the reversible change of the band intensities of HFB and LFB, suggesting the reversible formation of CO-stabilized Cu clusters containing under-coordinated Cu atoms. It is worth to note that while the sufficient detection of SERS effect usually requires roughening of copper surface, the use of silica encapsulated Au nanoparticles (Au@SiO_2), as inert surface signals amplifiers provides an effective strategy to conduct SERS investigations without the need to modify target surface morphologies.^{52, 53} Zhao et al.⁵⁴ applied this technique to monitor the single crystal low index Cu(*hkl*) surfaces on the CO_2RR in KHCO_3 solutions



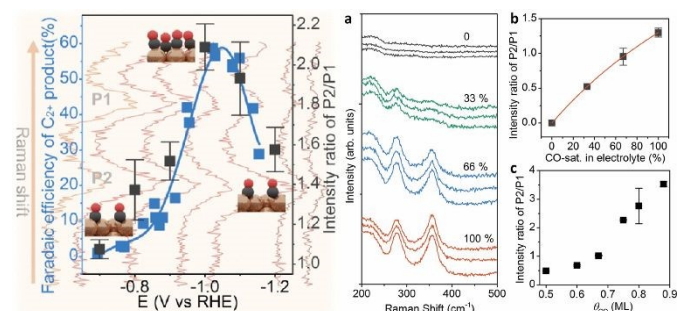
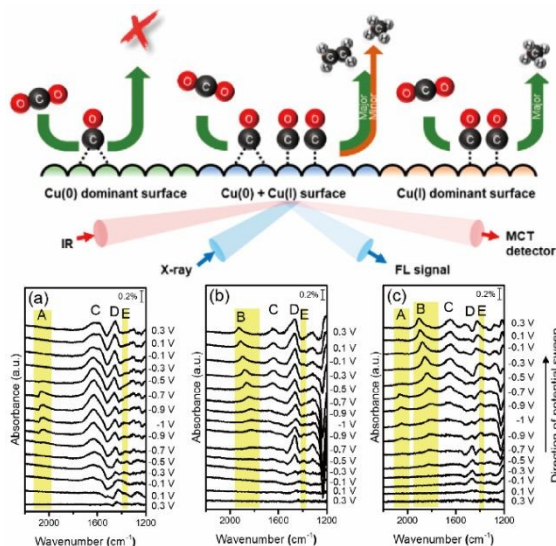


Figure 3. Left half: Correlation between potential-dependent intensity ratio of (P1:350cm⁻¹/ P2:280cm⁻¹) and Faraday efficiency of multi-carbon production showing volcano trend in the function of potentials. Right half: (a) Raman spectra of adsorbed CO on Cu with different CO concentrations in the 0.1 mol dm⁻³ KHCO₃ electrolyte. The experiments with different CO concentrations were repeated three times. (b) The intensity ratio of two peaks as a function of the CO concentration, where the red line shows the fitting result based on a Langmuir equation. (c) Theoretical benchmark of the peak ratio intensity vs CO coverage. Adapted with permission from ref 45. Copyright 2021 American Chemical Society.



peak label	peak position (cm ⁻¹)	assignments
A	1951–2094	CO stretching in atop-adsorbed CO
B	1806–1907	CO stretching in bridge-adsorbed CO
C	1645	H–O–H bending of H ₂ O
D	1467	C–O stretching of HCO ₂ ⁻
E	1396	COO ⁻ symmetric stretching

Figure 4. Upper row: Schematic diagram of the detection of the reaction selectivity and final products on Cu surfaces with different oxidation states using IR and X-ray spectroscopies. Middle row: *In situ* SEIRAS of the (a) electrodeposited Cu, (b) as-prepared Cu, and (c) CV-treated Cu electrodes during cathodic and anodic scans in CO₂-saturated 0.1 mol dm⁻³ KHCO₃ electrolyte solution. Lower row: Table shows the vibrational frequencies and assignments for the species in the IR spectra (a)-(c) under electrochemical CO₂RR. Adapted with permission from ref 46. Copyright 2020 American Chemical Society. Table 1 shows the vibrational frequencies and assignments for the species in electrochemical CO₂RR. Adapted with permission from ref 46. Copyright 2020 American Chemical Society.

using *in situ* Raman spectroscopy. The reaction intermediates such as *COOH, *CO, *OCCO and *CH₂CHO were observed depending on the surface-crystal structure that determined the reaction selectivity. Combining with theoretical calculations, Cu(111) facilitates the generation of C₁ products through the formation of intermediates *COOH and *CO, while Cu(110) further generates C₂ through the pathway of *OCCO and *CH₂CHO reaction intermediates.

3. Direct in situ observation of electrochemical CO₂RR on organically modified Cu surfaces

3.1 Inhibitory effects of molecular adsorption on active Cu sites

When introducing modifiers, the poisoning of active Cu sites owing to the adsorption of small molecules is a critical consideration. Although this phenomenon might be prevalent, it is often unreported because of activity losses. Waegle et al.⁵⁵ elucidated this phenomenon by comparing the influence of the adsorption of 1-(4-tolyl)pyridinium (T-Pyr)⁵⁶ and 1-(4-pyridyl)pyridinium (P-Pyr) on CO₂RR activity (Figure 5a). Surface modification with T-Pyr increased the production of C₂₊ compounds by increasing the interfacial pH. In contrast, surface modification with P-Pyr completely suppressed hydrocarbon production owing to the presence of the pyridine moiety (Figure 5b). Notably, the P-Pyr-modified surface produced comparable amount of hydrogen to the unmodified surface. SEIRAS analysis revealed the disappearance of the *CO_{atop} band (2070 cm⁻¹, * denotes the adsorbed species on the surface) attributed to the uncoordinated Cu sites on the P-Pyr-modified surface (Figure 5c). Conversely, the *CO_{atop} band at 2040 cm⁻¹, attributed to highly coordinated Cu sites, was observed for the T-Pyr- and P-Pyr-modified and unmodified surfaces. These results indicate that the competitive adsorption between the nitrogen in pyridine and CO inhibits the activity at low coordination sites.

Lv et al.⁵⁷ demonstrated that the modification using stearic acid was ineffective in any reduction process owing to its closely packed linear alkyl chain structure, whereas the sparser modification with aromatic group was effective for producing large amounts of C₂₊ products with good selectivity. Alkanethiols with long alkyl chain generally form closely packed, self-assembled monolayers on metal surfaces, causing significant poisoning. However, adsorbed alkanethiol can desorb when a cathodic potential is applied (reductive desorption). Fontecave et al.³² used the reductive desorption of alkanethiol to expose surface Cu atoms while maintaining high surface hydrophobicity, which was achieved by modifying both the morphology (Cu dendrites) and 1-octadecanethiol. Only the top tip of the dendrite interacted with the electrolyte, which electrochemically activated it at the site where the reductive desorption of 1-octadecanethiol occurred. This site, located at the triple-phase boundary (gas/electrolyte/copper), is advantageous for the formation of C₂₊ products, as featured in subsequent sections (3.3 and 3.4). Dai et al.⁵⁸ exploited alkanethiol in a similar phase-boundary strategy.



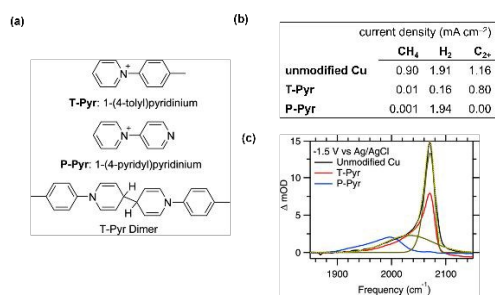


Figure 5. (a) Modifiers and reduced dimeric structure^{41,42} (b) CO₂RR Selectivity on Cu electrodes with 10 mM modifiers in CO₂-Saturated 0.1 M KHCO₃ at an Applied Potential of -1.1 V vs an RHE.⁴¹ (c) Comparison of the C≡O stretch bands of CO₂atop on Cu with different modifiers observed with SEIRAS at an applied potential of -1.5 V at the three different interfaces as indicated. The green dashed and solid lines represent a fit of the model. Reproduced with permission from ref 55. Copyright 2019 American Chemical Society.

Buonsanti et al.⁵⁹ introduced various surfactants on Cu nanocrystals and monitored their adsorption behaviour under cathodic potential. Dodecanethiol remained adsorbed on the nanocrystal surface and inhibited hydrocarbon production during CO₂RR, while the other ligands desorbed rapidly before the CO₂RR, exerting negligible influence on product distribution.

3.2 Specific surface interactions between the modifier and CO₂RR intermediates

Specific interactions between the introduced organic moieties and surface carbonaceous intermediates have been a primary focus since early studies, such as those by Verma et al.²⁷ using solid polymer electrolytes and Wang et al.²⁶ using amino acids for modification. The theoretical calculations further supported these findings^{28,29}. Etzold et al.⁶⁰ introduced the ionic liquid 1-butyl-3-methylimidazolium bis(trifluoromethylsulfonyl)imide ([BMIm][NTf₂]) as a chemical trapping agent. By analysing the product spectra under different conditions, the researchers elucidated the surface processes that led to the formation of multiple products on Cu. Although these studies demonstrated the effectiveness of organic modification and inspired subsequent research, direct observations of these reactions were not provided.

Recently, *in situ* vibrational spectroscopy has become common for probing molecular interactions during CO₂ reduction. Wang et al.⁶¹ introduced a 2,5-dimethoxy-1,4-benzoquinone (DMBQ) polymer onto a Cu surface (Figure 6a), which enhanced the current density and C₂₊ product selectivity (Figure 6c). The researchers attributed these improvements to the quinone groups, which facilitated CO₂ reduction via the reduction of the quinone moiety. *In situ* ATR-SEIRAS measurements detected a DMBQ-CO₂⁻ adduct peak at 1529 cm⁻¹ attributed to the vibration of the quinone ring skeleton in DMBQ. However, the 1582 cm⁻¹ band for unmodified Cu, attributed to the asymmetric stretching vibration of *CO₂⁻, was absent. They concluded that CO₂ was reduced to *CO via the formation of an adduct with the reduced quinone moiety without directly forming *CO₂⁻ on the Cu surface. The increased intensity of the *CO peak (Figure 6b) indicates a more efficient quinone-mediated reduction than

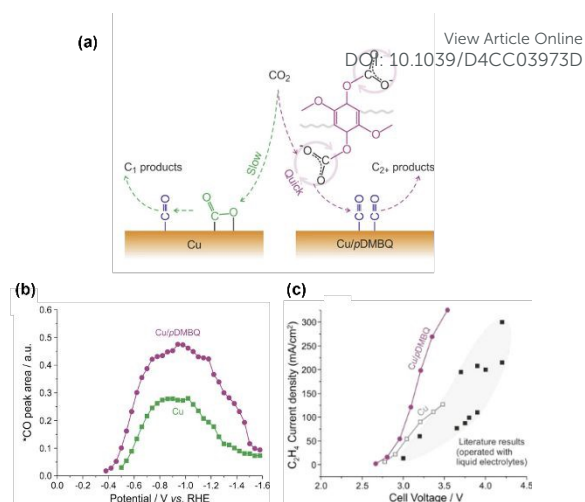


Figure 6. (a) Schematic illustration of CO₂ reduction over bare Cu (left) and Cu/pDMBQ (right) (b) Integral areas of *CO band at different potentials observed by ATR-SEIRAS for CO₂ reduction. (c) C₂H₄ partial current densities versus cell voltages for CO₂/pure water coelectrolysis using an MEA electrolyzer with the Cu/pDMBQ GDE (purple dot) and Cu GDE (gray open square). Reproduced with permission from ref 61. Copyright 2022 American Chemical Society.

direct CO₂ reduction, thereby increasing the probability of *CO forming C-C bonds and producing C₂₊ products (Figure 6a).

Lim et al.⁶² incorporated histidine into Cu₂O and deposited it on a carbon electrode. Among various imidazolium-based modifiers, histidine is particularly effective for the formation of C₂₊ products, especially ethanol. *In situ* Raman spectroscopy revealed that histidine was adsorbed physically onto the Cu surface and persisted throughout the CO₂RR, potentially owing to the formation of the carbamate cation via a CO₂ adduct, enabling it to remain stable on the electrode in a cathodic environment. Interestingly, the absence of the characteristic Cu-CO and C≡O frustrated rotation bands (typically observed at 279 and 364 cm⁻¹, respectively) indicated the absence of *CO, a common intermediate for C₂₊ products. Although the C≡O stretching vibration might have been obscured by a histidine-related band at 2081 cm⁻¹, the spectroscopic evidence and theoretical calculations prompted the researchers to propose a reaction mechanism that proceeded via a histidine-CO₂ adduct and not via *CO.

Fontecave et al.⁶³ reported that modification with 4-mercaptopyridine strongly favoured formate formation. Based on theoretical calculations, the researchers proposed a mechanism in which the modifier suppresses one of the initial CO₂ reduction pathways involving C-Cu bond formation, which typically leads to the formation of the *CO intermediate. Conversely, another pathway proceeding via O-Cu bond formation is unaffected and ends in formate formation. Interestingly, Liu et al.⁶⁴ reported that 4-mercaptopyridine significantly affected the reduction step of externally supplied CO, and the product was dominated by acetate. *In situ* ATR-SEIRAS analysis reveals increased amount of *CO_{bridge} upon modification. This *CO_{bridge} is more susceptible to being reduced to *CHO, which can then asymmetrically couple with *CO_{atop} to



form *OCCHO , a plausible intermediate for acetate formation. The detection of the *CHO and *OCCHO peaks further supported the proposed reaction pathway. The theoretical calculations indicated that 4-mercaptopyridine modified the local reaction environment of Cu and stabilised intermediates by forming hydrogen bonds through the nitrogen atom.

Liu et al.⁶⁵ introduced a common surfactant, dodecyl sulfonate, on the Cu surface by reducing dodecyl sulfonate-modified $Cu(OH)_2$. The catalyst exhibited high selectivity for C_{2+} product formation (86% Faraday efficiency (FE)), and particularly a high proportion of ethanol (64% FE) was formed. *In situ* Raman spectroscopy revealed a higher wavenumber for the Cu–CO stretching (362 cm^{-1}) for modified Cu than for unmodified Cu (354 cm^{-1}), which may indicate differences in reactivity. They also analysed the reaction intermediate *HCCOH , which can be converted into ethylene and ethanol. The peak at 1197 cm^{-1} was attributed to the stretching vibration of C–OH in the *HCCOH intermediate, whereas it appeared at 1182 cm^{-1} for the unmodified catalyst, indicating that the interaction with dodecyl sulfonate strengthened the C–O bond. This phenomenon can be attributed to hydrogen bonding between the dodecyl sulfonate anion and hydroxyl H of this intermediate. The stabilised C–O bonds is difficult to cleave, leading to the formation of ethanol.

3.3 Effect of modifiers on CO_2RR involving surface water molecules

Modification via the electrodimmerization of arylpyridinium on Cu (Figure 5a) is a well-established example of promoting CO_2RR via organic modification. When first reported by Agapie et al. in 2017⁵⁶, the role of organic modification was unclear. Waegeler et al.⁵⁵ elucidated the promotion mechanism using SEIRAS and observed an increase in the local pH of the modified electrode by monitoring the carbonate peaks in solution. Sargent et al.⁶⁶ exploited molecular design to expand this family of molecules by introducing substituents. By evaluating their performance, the researchers provided an explanation for CO_2RR promotion, which was supported by theoretical calculations and *in situ* spectroscopy. They determined the $^*CO_{atop}/^*CO_{bridge}$ ratio by *in situ* Raman spectroscopy and identified a volcano-type relationship between this ratio and the ethylene selectivity in CO_2RR . This finding indicates that the $^*CO_{bridge}-^*CO_{bridge}$ or $^*CO_{atop}-^*CO_{atop}$ pathway is responsible for efficient ethylene formation via the formation of C–C bonds between $^*CO_{atop}$ and $^*CO_{bridge}$. A linear relationship between the Bader charge of N in tetrahydro-bipyridine and $^*CO_{atop}/^*CO_{bridge}$ ratio was demonstrated, and an interaction model mediated by H_2O molecules was proposed.

Wang et al.⁶⁷ reported that modification with glutathione (Figure 7a) selectively formed methane from CO_2 , with minimal formation of C_{2+} products (Figure 7b). *In situ* Raman spectra (Figure 7c) indicated the absence of $^*CO_{atop}$, which is essential for C–C coupling and the formation of C_{2+} products. They also used the bicarbonate/carbonate peak ratio to indicate surface pH. A larger bicarbonate/carbonate peak ratio for glutathione-modified Cu indicated a lower local pH, possibly owing to the affinity of deprotonated carboxylate anion (COO^-) for H_2O ,

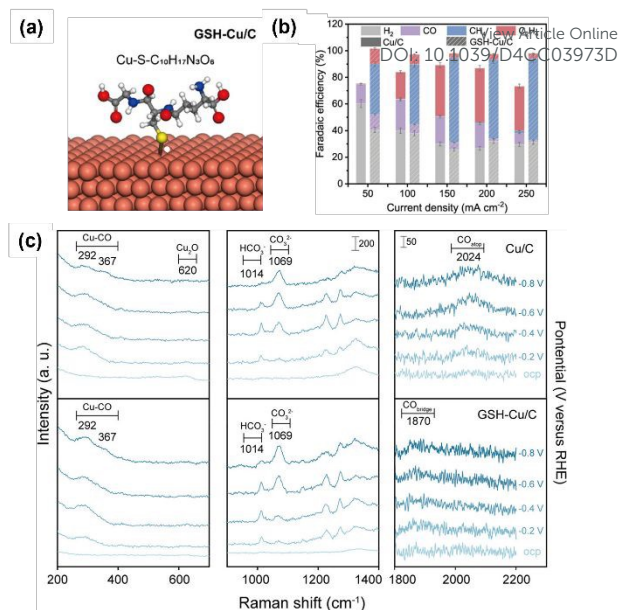


Figure 7. (a) Structure of modified Cu with glutathione (GSH). (b) Effect of GSH modification on CO_2RR product (c) Operando Raman spectra for Cu/C and GSH-Cu/C at a potential range of OCP $\sim -0.8\text{ V}$ vs RHE. Reproduced with permission from ref 67. Copyright 2022 American Chemical Society.

which promoted proton release. This proton supply effect can also facilitate further reduction of *CO to methane before C–C bond formation and C_{2+} product generation.

Toma et al.³⁰ also modified a library of organic molecules and polymers and classified the modifiers based on their protic/aprotic substituents and hydrophobicity. A comparison of the products of CO_2RR under mild potential indicated that the products were limited to H_2 , CO , and formate. Protic functional groups promoted the HER. The contact angle of the surface exhibited a good relationship with the formic acid ratio and was insensitive to the chemical nature of the modifier. This finding indicates that the modifiers indirectly influenced the CO_2RR by altering the behaviour of water on the surface. Adsorbed hydrogen is more stable on a hydrophobic surface than on a hydrophilic surface. The less stable adsorbed hydrogen can form H_2 or react with CO_2 to form formate; this process is more difficult on hydrophobic surfaces that produce CO as the major product. Although this study was not supported by *in situ* spectroscopic analysis, it indicated that the behaviour of surrounding water molecules significantly affects the CO_2RR , which can be modulated by surface molecular modifiers.

Cui et al.⁶⁸ observed surface water molecules on a hydrophobic octadecanethiol-modified Cu electrode using *in situ* Raman spectroscopy. The OH stretching band was deconvoluted into three peaks (Figure 8a) corresponding to tetrahedrally coordinated H-bonded water at approximately 3200 cm^{-1} , trigonally coordinated H-bonded water at approximately 3400 cm^{-1} , and H-bonding-free water with dangling O–H bonds at approximately 3600 cm^{-1} . The



unmodified Cu electrode showed a strong dependence of the ratio of these components on the applied potential, with the

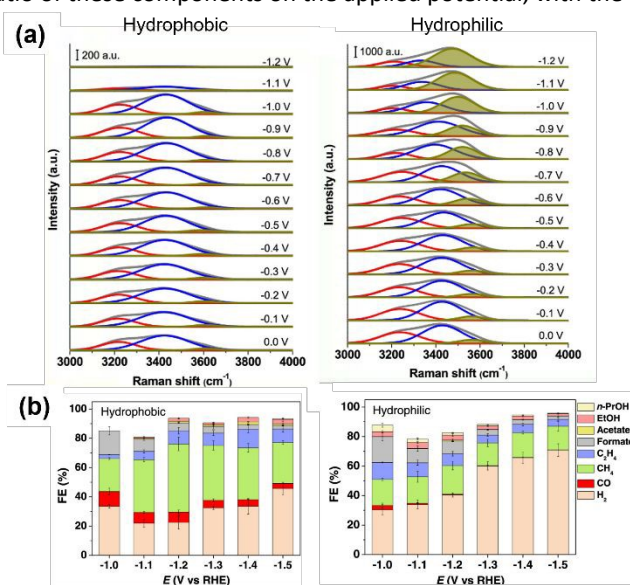


Figure 8. (a) *In situ* Raman spectra of the O–H stretching mode of interfacial water molecules with (Hydrophobic) and without (Hydrophilic) modification with 1-octadecanethiol. Peaks are deconvoluted. (b) Effect of modification on CO₂RR selectivity. Reproduced with permission from ref 68. Copyright 2021 American Chemical Society.

amount of free water increasing as the potential became more negative. This finding indicates that the applied potential caused the water molecules to adopt two H-down configurations, cleaving the hydrogen-bond network among the surface water molecules and causing the water to dissociate into *H. In contrast, the hydrophobic octadecanethiol-modified Cu surface exhibited a relatively smaller OH stretching band, and the OH band was almost insensitive to the applied potential. This phenomenon leads to a lower tendency for surface *H formation. They also observed a *CO stretching band, indicating that the modification promoted *CO formation and enhanced its adsorption. This observation explains the performance of modified surfaces in CO₂RR, suppression of HER, and increase in methane formation (Figure 8b).

Zheng et al.⁵⁷ modified CuO nanosheets with toluene (T-Cu) via catalytic aerobic oxidation. The distance between immobilised toluene moieties on the Cu surface (5.1 Å) indicated a more dispersed structure of the hydrophobic surface than stearic acid-modified Cu surface (S-Cu). Analysis of surface water molecules using *in situ* Raman spectroscopy indicated that the O–H stretching band of water could be deconvoluted into three peaks: 4-coordinated hydrogen-bonded water at approximately 3200 cm⁻¹ (4-HB·H₂O), 2-coordinated hydrogen-bonded water at approximately 3400 cm⁻¹ (2-HB·H₂O), and K⁺ ion-hydrated water at approximately 3600 cm⁻¹ (K·H₂O) (Figure 9d). The increasing peak ratio for the K·H₂O component with a more negative potential indicated the cleavage of hydrogen bonds and coverage of the surface by *H. It increased steeply for

unmodified Cu; however, the increase was moderate for the toluene-modified catalyst (Figure 9e). For closely packed S-Cu,

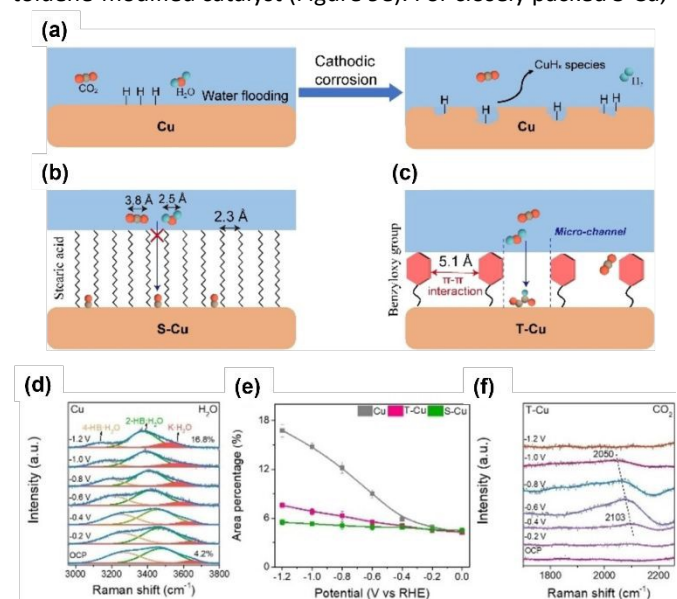


Figure 9. Schematic presentation of surface processes for (a) unmodified Cu (b) Cu modified with stearic acid (S-Cu) (c) Cu modified with benzoyloxy group (T-Cu). (d) *In situ* Raman spectra of the interfacial water structure on Cu from 0 to -1.2 V. Peaks are deconvoluted. (e) Area percentages of K·H₂O peaks at different applied potentials on Cu, T-Cu and S-Cu. (f) *In situ* Raman spectra of the CO adsorption peak on T-Cu. Reproduced with permission from ref 57. Copyright 2023 Wiley.

the increase was the smallest. The difference in the behaviour of surface water was reflected in the CO₂RR performance, with unmodified Cu producing a large amount of hydrogen (Figure 9a), S-Cu consuming minimal total current for CO production (Figure 9b), and T-Cu exhibiting the most efficient formation of C₂₊ products while suppressing hydrogen formation (Figure 9c). These results indicate that maintaining the space between modifiers for effective proton transport and CO–CO dimerisation is essential for modifiers (Figure 9f).

The strategy of introducing a molecular layer is a general method for decreasing HER. Lu et al.⁶⁹ studied the CO₂RR under high-pressure CO₂ conditions. Under these conditions, the carbonaceous product was converted to formate; however, some H₂ was still produced. They introduced polypyrrole as a proton-resistant layer and succeeded in reducing H₂ production.

Thoi et al.⁷⁰ reported that the addition of a small amount of an ammonium surfactant (cetyltrimethylammonium bromide, CTAB) significantly suppressed HER. The CO₂RR performance is affected by the type of alkali cation in the electrolyte^{71,72} owing to the presence of surrounding hydrated water molecules. The addition of CTAB mitigated the difference between these alkali cations, decreasing HER and increasing CO and formate formation. ATR–SEIRAS measurements revealed a decrease in the intensity of the O–H stretching band of surface water, which was also insensitive to the applied negative potential. This phenomenon can be attributed to the substitution of hydrated alkali cations with CTA⁺ cations, which led to the suppression of



HER. However, the disruption of the interaction between the hydrated cation and reaction intermediate also resulted in the

inhibition of the pathway for C_{2+} product formation, with CO and formate being the major products.

The influence of CTAB on the CO_2 RR on Cu was also studied by Wang et al.,⁷³ who revealed that formate formation was strongly increased in the low overpotential region (-0.5 V vs. RHE, Figure 10a). *In situ* Raman spectroscopy revealed a band centred at approximately 2900 cm^{-1} attributed to C–H stretching in $HCOO^*$, which is an intermediate for formate formation (Figure 10b). The reductive desorption of $HCOO^*$ as formate can be considered a rate-determining step. They observed a change in the shape of this band (Figure 10c), which was attributed to the substitution of $HCOO^*$ with CTA^+ at surface. Because cationic CTA^+ is attracted as the potential shifts to negative values, the reductive desorption of $HCOO^*$ is promoted, resulting in a 56-fold increase in formate formation with 86% selectivity in this low-overpotential region.

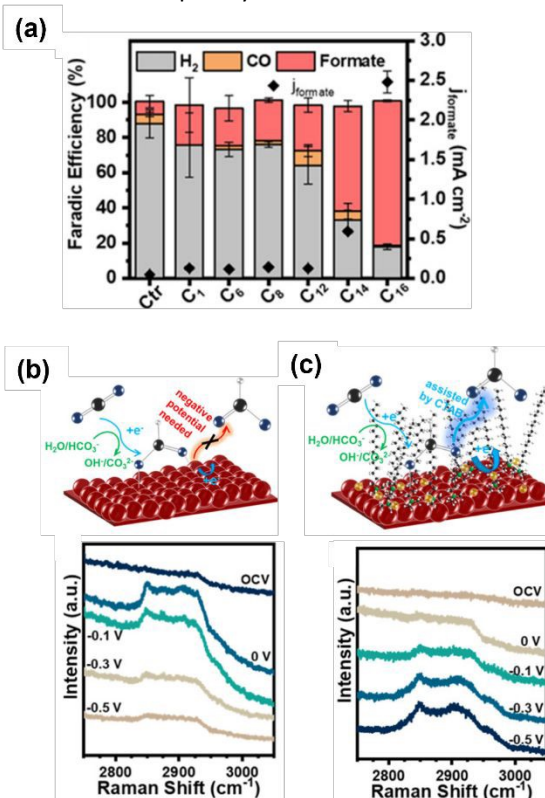
Surentharath et al.⁷⁴ analysed the electrochemical kinetics of the CO_2 RR in an aprotic solvent, dimethylsulfoxide (DMSO), with phenol as a proton donor, indicating that different proton transfer processes significantly directed the reaction towards C_{2+} production. Jiao et al.⁷⁵ studied the synergistic effect of DMSO, a hydrated alkaline cation. They primarily used constant-potential *ab initio* molecular dynamics simulations to explain the synergistic effect between the cation (Na^+) and aprotic solvent (DMSO) in the electrolyte, resulting in an improvement in C_{2+} selectivity. The synergistic effect significantly reduced the connectivity of the water network, reducing the HER and formation of the C_1 precursors $*COH$ or $*CHO$, without affecting the hydrogenation of $*OCCO^*$. These predictions were experimentally validated using *in situ* ATR-IR spectroscopy, which revealed more prominent $*OCHO$ and $*OCCOH$ with DMSO addition, even under a moderate potential of -0.3 V vs. RHE. This finding corroborates their prediction that C–C bond formation is favoured by the environment provided by the cation and aprotic solvent.

3.4 Effect of modification on the transportation of CO_2 , H_2O , and protons

The poor solubility of CO_2 molecules in water limits the intrinsic activity of Cu catalysts. In addition to the amount of CO_2 consumed in the CO_2 RR process, the decomposition of CO_2 into bicarbonate and carbonate anions under high local pH conditions is easily achieved by cathodic electrolysis. Excess water in CO_2 also leads to a loss of electrical energy in the HER. In addition, the sparse adsorption of $*CO$ tends to reduce the probability of C–C bond formation. The application of gas diffusion electrode (GDE) in a flow cell, which directly introduces gaseous CO_2 onto the electrode surface, significantly increases the geometric partial current density for C_{2+} products by one order of magnitude, from several 10 to 100 mA cm^{-1} . Even when the catalyst surface is completely immersed in an aqueous electrolyte, the selective transport of CO_2 except H_2O at the

microscopic level is expected to improve the production of C_{2+} products.

Alkanethiols are frequently used modifiers due to their fairly



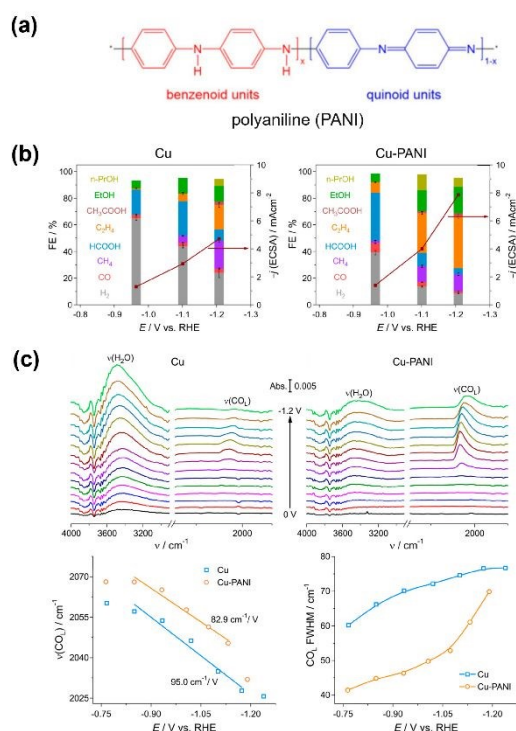
stable adsorption even under CO_2 RR operation. We already

Figure 10. (a) Dependence of the electrocatalytic CO_2 reduction performance of Cu on straight-chain alkyl group R of the $NR(CH_2)_3Br$ additive. (b)(c) *In situ* Raman spectra of Cu and Cu-CTAB in the CO_2 -saturated 0.5 M $KHCO_3$ under applied potentials, with schematic illustration formate formation. Reproduced with permission from ref 73. Copyright 2020 American Chemical Society.

discussed their effect in Section 3.1 and 3.3, and they also significantly affect the CO_2 and H_2O transportation onto the surface. Gong et al.⁷⁶ systematically changed the length of alkyl chain in alkanethiol modifiers and showed that stronger hydrophobicity with octadecanethiol enhanced CO_2 mass transport, while shorter dodecanethiol can make the most efficient gas-liquid-solid contact affording large current density. They used *in situ* fluorescence electrochemical microscopy to evaluate local CO_2/H_2O ratio under CO_2 RR operation, which corresponds to the ratio of $*CO$ and $*H$. The ratio of these adsorbed species does not only influence the HER process but also the reaction branching between ethanol and ethylene.

Luo et al.⁷⁷ compared different polymer binders for a needle-like CuO catalyst ink with different hydrophobicities (polyacrylic acid (PAA), Nafion, and fluorinated ethylene propylene (FEP)). Among the three binders, FEP exhibited the highest selectivity and current density of C_{2+} products. An evaluation of CO_2 -philicity and hydrophilicity by contact angle measurements indicated that the CO_2/H_2O ratio was the highest after modification with FEP. *In situ* Raman spectroscopy revealed that a high CO_2/H_2O ratio with the FEP binder corresponded to a wider potential range in which CO stretching was observed.





Zhuang et al.⁷⁸ introduced polyaniline (PANI) onto the Cu surface (Figure 11a), anticipating that the NH group in PANI has an affinity for CO₂. This modification increased the current

Figure 11. (a) Structure of PANI. (b) Modification effect on CO₂RR (c) (top) *In situ* ATR-SEIRAS spectra of CO₂RR on the Cu and Cu-PANI electrode, respectively, in CO₂ saturated 0.1 M KHCO₃. (bottom) Stark effects of the linearly adsorbed CO (CO_L) and full width at half-maximum (FWHM) of CO_L signals. Reproduced with permission from ref 78. Copyright 2020 American Chemical Society.

density of the C₂₊ products with high selectivity, indicating that a substantial amount of CO₂ was increased on the Cu surface (Figure 11b). They did not detect any differences in the Cu morphology or electronic state upon modification. The *in situ* ATR-SEIRAS measurements showed that the peak attributable to *CO_{atop} became more prominent relative to the OH stretching in H₂O at the surface upon modification (Figure 11c, top). They provided a more precise analysis of the *CO_{atop} stretching band (Figure 11c, bottom). They revealed a greater *CO stretching wavenumber and weak Stark effect, indicating weaker Cu-C interactions, possibly because of close *CO packing. The narrow bandwidth of *CO also led the researchers to conclude that the modification caused an increased production of *CO, which must be packed in an ordered geometry.

Daasbjerg et al.⁷⁹ studied the electrochemically deposited 1,1'-di-p-tolyl-1,1'-,4,4'-bipyridine (T-bipyridine) on polycrystalline Cu. The thickness of the deposited film was varied by varying the applied potential during electrodeposition. As the thickness of the organic film increased, the selectivity of ethylene increased. They used *in situ* Raman spectroscopy and observed a notable difference in the wavenumber of *CO stretching between the modified and unmodified surfaces, with the former exhibiting a higher intensity. They concluded that the

modification did not induce local reactivity on Cu, and greater *CO coverage was responsible for the increased production of C₂₊ products, which was significantly affected by the film thickness and porosity, and proposed that the higher CO partial pressure facilitated by the modification was a more significant factor than the surface hydrophobicity.

Xie et al.⁸⁰ proposed that an anti-swelling anion exchange ionomer (AEI) could optimise the local environment for the electroreduction of CO₂ to C₂₊ products at industrially relevant current densities on oxide-derived Cu. Unlike proton exchange ionomers, which typically have SO₃⁻ groups, AEI can accumulate OH⁻ via -N(CH₃)₃⁺ group while preventing excessive water from intruding onto the Cu surface (Figure 12a). The surface pH was estimated from the relative peak intensity of HCO₃⁻/CO₃²⁻ (Figures 12b and c), revealing that the modification with AEI increased the pH of the Cu surface at a high current density. *In situ* Raman spectroscopy revealed the presence of *OH, Cu-CO, and *CO, whereas *in situ* FTIR spectroscopy revealed the presence of *CO, HCO₃⁻, and COCO*. Based on these observations and theoretical calculations, they concluded that the increased surface pH facilitated the hydrogenation of COCO*.

Daasbjerg et al.⁸¹ analysed several polymer coatings of CuO electrodes and observed that the surface hydrophobicity of these polymers suppressed HER. They also suggested that an increase in surface pH with restricted water diffusion could promote ethylene formation.

These effects on the transport of organic modifiers works in assembling high-current-density electrolysis cells. Introducing hydrophobic polymers to create a triple-phase catalyst surface, where the CO₂ gas, electrolyte, and Cu surface meet at the active site, is extremely effective for increasing the current density for the formation of C₂₊ products.³³

3.5 Effect of modification on the charged state and structure of surface Cu

Zhao et al.⁸² introduced fullerene (C₆₀) onto CuO nanospindles. Because C₆₀ is known to be a good electron acceptor, it reserves electrons under cathodic potential and stabilises the Cu⁺ state of nearby surface Cu atoms (Figure 13a). The persistent Cu⁺ state under negative potential was monitored by *in situ* Raman spectroscopy (Figure 13b). Modification with C₆₀ significantly increased the formation of C₂₊ products (Figure 13d) while suppressing HER. The active surface was also monitored by *in situ* Raman spectroscopy (Figure 13c). A persistent, higher-wavenumber peak corresponding to *CO_{atop} appeared, indicating a smaller electron donation from Cu⁺ to *CO. They also observed the reduction intermediates *CHO (1700 cm⁻¹) and coupled *CO-CHO (1580 cm⁻¹), which were only successfully detected on the C₆₀-modified surface by *in situ* Raman spectroscopy and ATR-SEIRAS. Together with the theoretical calculations, they concluded that the preferential formation of *CHO and its reaction with *CO to form *CO-CHO provides an effective route for producing C₂₊ products.

Recently, metal surface modification with N-heterocyclic carbene ligands has been investigated as a powerful tool for



enhancing catalytic activity through strong interactions with surface metal atoms. Rosas-Hernández et al.⁸³ electrodeposited Cu nanoparticles onto Cu foil in the presence of *N*-heterocyclic

carbene-carbodiimide (NHC-CDI). This modification significantly increased the selectivity and current density of the carbonaceous products, and the performance showed a volcano-type dependence on the degree of modification. *In situ* Raman spectra showed that the *CO formed on the surface of unmodified Cu was mostly *CO_{bridge}, however, *CO_{atop} was formed exclusively on the modified surface. Close inspection of the *CO_{atop} peak revealed that Cu modified with a moderate amount of NHC-CDI, contained two components, each assigned to *CO coordinated on terrace sites (LFB) or step sites (HFB). HFBs disappeared with increasing amounts of modifier, possibly because of the occupation of the step site with the NHC-CDI ligand. These results indicate that HFB was more readily dimerised and explain the superior CO₂RR efficiency with moderate modification.

Chen et al.⁸⁴ highlighted the facet-stabilising effect of 1-dodecanthiol. As described previously^{32, 68}, modification with alkanethiol facilitated CO₂ transportation and *CO accumulation on the Cu surface. They prepared nanostructured CuO treated with 1-dodecanthiol and observed the intense peak of *CO for the modified surface in the *in situ* Raman spectrum, which agreed with previous reports. In addition, the slightly lower wavenumber at negative potentials indicated stronger CO binding on the modified surface. They conducted other *in situ* measurements to elucidate that the modified surface was more prone to be reduced to expose of the (100) plane of Cu. *In situ* ATR-FTIR spectroscopy exhibited a resemblance of the *CO state on the modified surface to Cu(100) and the unmodified surface to Cu(111). The intermediates *CHO and *CO-CHO were only observed on the modified surface, and theoretical calculations predicted that the C-C bond formation pathway from *CHO to *CO-CHO was favoured on the Cu(100) surface.

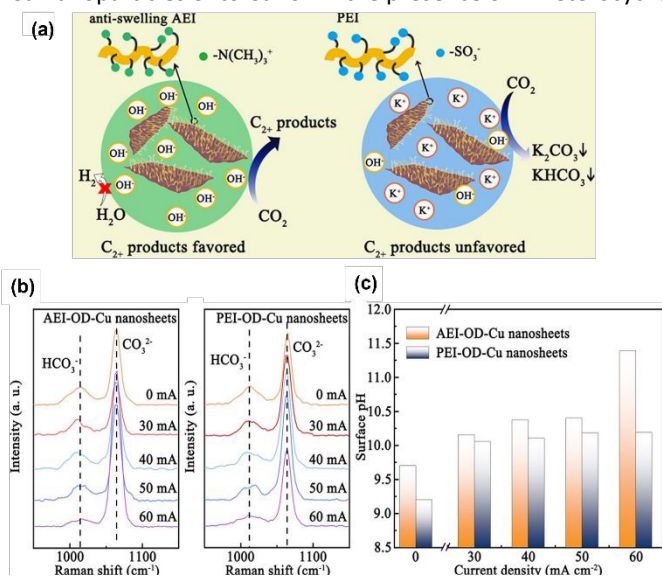


Figure 12. (a) Schematic illustration of CO₂-to-C₂₊ activity and selectivity through local environment construction. (b) *In situ* Raman spectra obtained from the AEI-OD-Cu and PEI-OD-Cu nanosheets. (c) pH values calculated from the *in situ* Raman spectra. Reproduced with permission from ref 80. Copyright 2022 American Chemical Society.

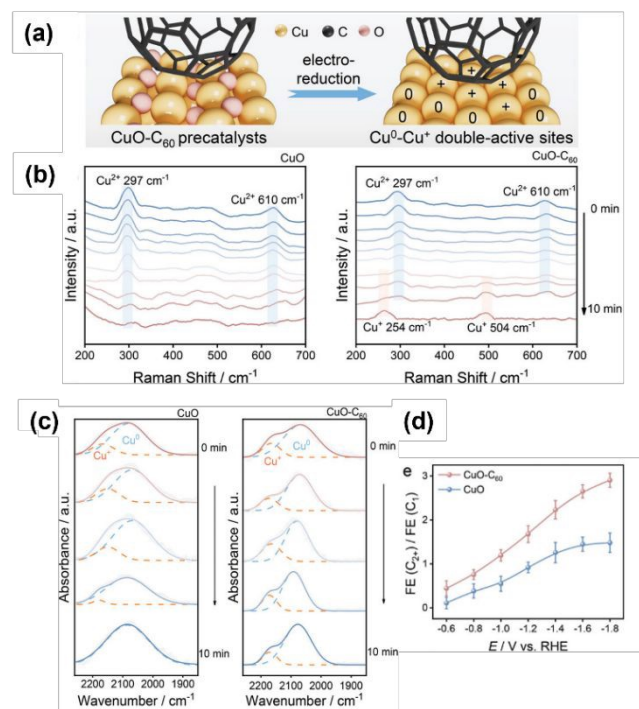


Figure 13. (a) Schematic illustration of the electroreduction of CuO-C₆₀ precatalysts. (b) *In situ* Raman spectra of CuO and CuO-C₆₀ precatalysts at a reduction potential of -0.4 V versus RHE. (c) *In situ* ATR-FTIR spectra under continuous CO₂ flow over CuO and CuO-C₆₀. (d) The Faraday efficiency ratios of C₂₊ to C₁ products from CO₂RR. Reproduced with permission from ref 82. Copyright 2023 Wiley.

4. New fabrication method for organic modifiers/Cu contact surfaces

In the previous sections, we reviewed the multifaceted effects of organic structures on the CO₂RR activity on Cu surfaces and role of *in situ* vibrational spectroscopy in monitoring surface events. Based on this understanding, it is evident that the fabrication method for creating an organic/Cu contact surface significantly affects the CO₂RR performance of the modified surface. Historically, modification was achieved using simple procedures, such as i) casting a modifier solution onto the Cu catalyst surface and ii) mixing the modifiers into the catalyst ink solution and depositing them onto the substrate surface. However, recent studies have shown that CO₂RR performance of modified surface can be significantly improved by employing methods to control the structure built on the surface.

Electrodeposition can modify the catalyst surface while maintaining its electroactivity because it does not function when the surface becomes electrochemically insulating owing to excessive deposition. It can also be used to introduce



modifiers with poor solubility or high tendency to aggregate, which make them difficult to be processed directly. Agapie et al.⁵⁶ used electrodeposition to deposit neutral dimers by reducing water-soluble *N*-arylpiperidinium salts across various piperidinium families. They also employed electrografting to covalently bond monomeric organic species, which enhanced the CO₂RR activity towards C₂₊ products.⁸⁵ Daasbjerg et al.⁷⁹ reported that although the reduced *N*-arylpiperidinium dimer is soluble in organic solvents, dissolving the electrodeposited film in acetone followed by complete drying diminished its effectiveness for the formation of C₂₊ products, owing to the transformation of the porous film into a closely packed structure. This result demonstrates the importance of the porous structure formed during electrodeposition for improving the catalytic activity of molecular films.

Restructuring the Cu surface by modification significantly influences the surface activity. During the cathodic dimerisation of *N,N*-ethylene-phenanthroline dibromide, Agapie et al.⁸⁶ observed a cubic structure on the Cu surface. The incorporation of halogenide anions into Cu promotes Cu restructuring, resulting in the increased production of C₂₊ products during the CO₂RR.⁸⁷ This process was accompanied by the deposition of organic films via the reductive dimerisation of *N,N*-ethylene-phenanthroline (Figure 14). The modified organic film played a dual role in enhancing the production of C₂₊ products: providing a preferential molecular reaction site,⁶⁶ and protecting cubic nanostructures with exposed {100} facets, which promoted the production of C₂₊ products but were unstable without protection.

The protective effect of the organic layers on nanostructured Cu was also investigated in a study on the effect of the size of the Cu nanoparticles. Similar to other metal nanoparticle catalysts, the size of Cu nanoparticles affects the electrochemical CO₂RR.⁸⁸⁻⁹⁰ In addition to the dispersed electronic state and number of low coordination sites in the nanoparticle state, C₂₊ formation in CO₂RR involved C–C bond formation, which was disadvantageous for subnanometer-sized particles with few cooperating surface atomic sites. Duan et al.⁹¹ investigated organic structures to elucidate the effect of Cu size. They simultaneously generated Cu⁰ and a graphdiyne scaffold by reacting an unstable copper (I)- σ -alkynyl complex at elevated temperatures (Figure 15). The Cu species were kinetically trapped in the graphdiyne scaffold, and the size of the particles was controlled by the amount of cuprous precursor, ranging from single-atomic Cu sites to nanoclusters. They observed a very clear dependence of the C₁/C₂₊ product ratio on particle size, predominantly forming C₁ products at single-atom sites and C₂₊ products at 1–1.5-nm-sized particles.

Recently, we developed a novel method for modifying catalytically active Cu surfaces.⁹²⁻⁹⁴ Cu-catalysed azide–alkyne cycloaddition (CuAAC) is a representative click chemistry technique that involves the formation of rigid covalent bonds between ethynyl and azide moieties. A distinctive aspect of this reaction is that Cu(I) is particularly active, with various Cu(I) species, salts, coordination compounds, and even insoluble inorganic solids known to catalyse this reaction. Initially, the metallic Cu electrode was electrochemically activated by

anodisation to catalyse CuAAC between monomeric azides and ethynyl species (Figure 16a). Although the reaction of these two monomers in solution afforded insoluble polymers that were

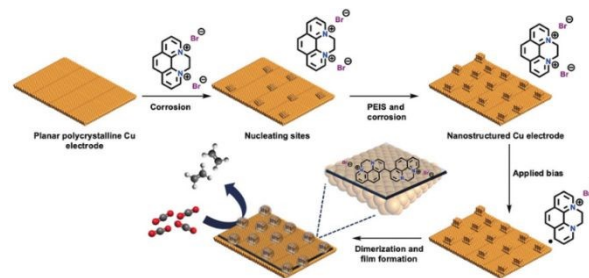


Figure 14. Pictorial representation of the model for nanostructuring of a polycrystalline copper electrode and film electrodeposition by dimerization of *N,N'*-ethylene-phenanthroline dibromide. The combination of film and nanostructuring leads to high C₂₊ selectivity for CO₂RR electrocatalysis. Reproduced with permission from ref 86. Copyright 2019 Wiley.

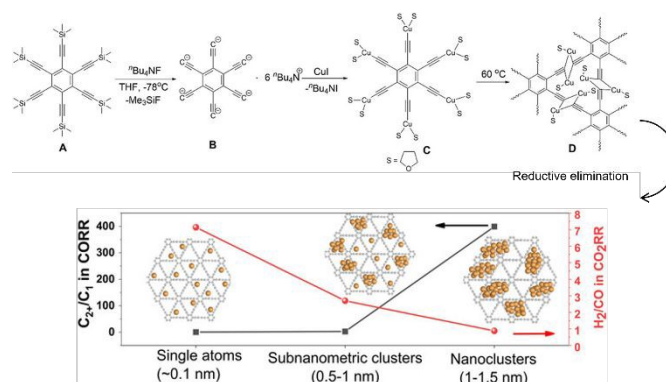


Figure 15. Schematic illustration for the synthesis of Cu/graphdiyne scaffold and size effect of Cu(0) catalysts on CO₂RR selectivity. Reproduced with permission from ref 91. Copyright 2022 Wiley.

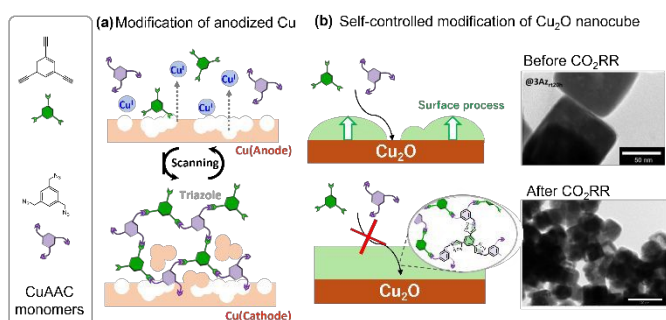


Figure 16. Schematic illustration of two CuAAC modification, on anodized Cu (a) and on Cu₂O nanocube, with TEM images of structural transformation upon CO₂RR (b). Reproduced with permission from ref 93 and 94. Copyright 2022 Wiley.

difficult to process, anodisation of the Cu electrode effectively deposited the polymer. This modification resulted in the increased production of C₂₊ products with the effective inhibition of the HER⁹². The modification with a small triazole molecule resulted in the inhibition of the CO₂RR, demonstrating



the importance of structural design beyond the kind of molecular groups. The feasibility of CuAAC also enabled the evaluation of different molecular moieties incorporated in the modified layer to demonstrate the special effect of tertiary amine moieties, which are effective proton carriers in the modified layer⁹³. We subsequently investigated layer growth from the same component on nanocrystalline Cu₂O without electrochemical stimulation (Figure 16b)⁹⁴. The resulting layer on Cu₂O was extremely flat and thin. An important feature of this method is that the layer growth point is fixed on the surface Cu(I) of Cu₂O, thus rendering the growth self-regulating by preventing the further approach of the monomer on the Cu₂O surface. The layer structure was independent of the surface Cu(I) activity but reliant on the degree of modification of the layer growth, leading to the formation of a uniform layer. Although the layer thickness was only a few nanometres, it effectively inhibited HER. Another important feature of this modification is protecting effect. Cu₂O was mostly reduced to a Cu(0) species without losing its initial cubic structure. Transmission electron microscopy revealed that Cu₂O was reduced within the formed layer, forming a hollow at the centre to compensate for the volume decrease (Figure 16b). These results further motivated us to investigate the control of the structure of organic/Cu contact surfaces, where Cu exhibits a dynamic structure during catalysis.

5. Conclusions and Outlook

Many studies have demonstrated the efficacy of organic modifiers on the activity of CO₂RR on Cu electrocatalysts, particularly in the production of C₂₊ products. With the progress in understanding general Cu electrocatalysts, the roles of organic modifiers should be examined from various perspectives. First, the diverse product range of the CO₂RR on copper complicates reaction pathway elucidation compared to other cathodic electrocatalysts, as reaction conditions exert a greater influence on product formation. Second, the governing factor of the reaction is significantly different from that of homogeneous molecular catalysts, in which activity is primarily understood by considering the nearest molecular interactions. Additionally, CO₂ electrolysis relies on the transport of poorly soluble CO₂ to water and other proton suppliers. Therefore, making the surface hydrophobic or creating a triple-phase boundary can improve the CO₂RR performance. These aspects underscore the importance of direct *in situ* observation of the Cu surface during catalysis to better understand the role of the modifiers.

This article collects the studies of the analysis of a Cu catalyst modified with organic compounds using *in situ* vibrational spectroscopy to classify the role of the organic modifiers. This technique enables the visualisation of the reduction intermediates, such as *CO, and reveals the states of water and Cu, which are important for understanding the effects of the modifiers. In addition, these bands can serve as indicators of local pH and electric field, providing extensive information about the key factors influencing CO₂RR. A deeper

understanding of these methods will significantly facilitate research in this field.

DOI: 10.1039/D4CC03973D

The method of fabricating organic/Cu contact surfaces has significant potential for improving the CO₂RR performance. We have highlighted successful examples in which the fabrication procedure was crucial for demonstrating the potential of the modifier. In addition, Cu exhibits a dynamic structure during electrocatalysis, which is significantly affected by the presence of modifiers that act as surface stabilisers. We discussed some of these studies, including our recent efforts to develop a new fabrication method in which Cu is not merely modified but actively participates in the modification process. The active participation of Cu leads to precisely controlled contact surface modification, the accumulation of more active Cu atoms on the surface, and the fabrication of effective and selective mass transport routes.

The designability of molecular modifiers has been expected to be a powerful tool for efficient and selective electrochemical CO₂ conversion into various chemicals on copper. The development of electrochemical CO₂RR on copper revealed the importance of the total designing of an electrochemical system, from the atomic scale to the interface structure and the whole cell assembly, which entangle one another. The enhancement of local activity can cause local CO₂ depletion more easily, and it inevitably requires further improvement in CO₂ transport. Also the works summarized in this review showed that a single molecular modifier can have multiple wide-ranging effects. The application of *in situ* vibrational spectroscopy is indispensable in dissecting these tangled factors. It can also provide important clues in designing molecular modifiers integrated with copper atom assembly, toward selective and effective production of a specific product among various optional chemicals from CO₂.

Conflicts of interest

There are no conflicts to declare.

Data availability

No primary research results, software or code have been included and no new data were generated or analysed as part of this review.

Acknowledgements

This study was financially supported by KAKENHI (grant no. 22K05129 and 21K05125) from Japan Society for the Promotion of Science (JSPS). AK acknowledges for the financial support from the Cooperative Research Program of "Network Joint Research Center for Material and Devices" and the Ogasawara Memorial Foundation.

References

- 1 M. E. Royer, *Comptes Rendus Acad. Sci.*, 1870, **70**, 731-732.
- 2 L. V. Haynes, D. T. Sawyer, *Anal. Chem.*, 1967, **39**, 332-8.
- 3 Y. Hori, H. Wakebe, T. Tsukamoto, O. Koga, *Electrochim. Acta*, 1957, **39**, 1833-9.



- 4 Y. Hori, K. Kikuchi, S. Suzuki, *Chem. Lett.*, 1985, 1695-8.
- 5 Y. Hori, K. Kikuchi, A. Murata, S. Suzuki, *Chem. Lett.*, 1986, **0**, 897-8.
- 6 C. W. Li, M. W. Kanan, *J. Am. Chem. Soc.*, 2012, **134**, 7231-7234.
- 7 C. W. Li, J. Ciston, M. W. Kanan, *Nature*, 2014, **508**, 504-507.
- 8 H. Mistry, A. S. Varela, C. S. Bonifacio, I. Zegkinoglou, I. Sinev, Y.-W. Choi, K. Kisslinger, E. A. Stach, J. C. Yang, P. Strasser, B. R. Cuenya, *Nat. Commun.*, 2016, **7**, 12123.
- 9 C. Liu, M. P. Lourenco, S. Hedstroem, F. Cavalca, O. Diaz-Morales, H. A. Duarte, A. Nilsson, L. G. M. Pettersson, *J. Phys. Chem. C*, 2017, **121**, 25010-25017.
- 10 W. Zhang, C. Huang, Q. Xiao, L. Yu, L. Shuai, P. An, J. Zhang, M. Qiu, Z. Ren, Y. Yu, *J. Am. Chem. Soc.*, 2020, **142**, 11417-11427.
- 11 P. Qi, L. Zhao, Z. Deng, H. Sun, H. Li, Q. Liu, X. Li, Y. Lian, J. Cheng, J. Guo, Y. Cui, Y. Peng, *J. Phys. Chem. Lett.*, 2021, **12**, 3941-3950.
- 12 R. G. Mariano, K. McKelvey, H. S. White, M. W. Kanan, *Science*, 2017, **358**, 1187-1192.
- 13 Y. Yang, S. Louisiana, S. Yu, J. Jin, I. Roh, C. Chen, M. V. Fonseca Guzman, J. Feijoo, P.-C. Chen, H. Wang, C. J. Pollock, X. Huang, Y.-T. Shao, C. Wang, D. A. Muller, H. D. Abruna, P. Yang, *Nature*, 2023, **614**, 262-269.
- 14 Q. Lei, H. Zhu, K. Song, N. Wei, L. Liu, D. Zhang, J. Yin, X. Dong, K. Yao, N. Wang, X. Li, B. Davaasuren, J. Wang, Y. Han, *J. Am. Chem. Soc.*, 2020, **142**, 4213-4222.
- 15 M. R. Singh, Y. Kwon, Y. Lum, J. W. Ager, A. T. Bell, *J. Am. Chem. Soc.*, 2016, **138**, 13006-13012.
- 16 P. Grosse, D. Gao, F. Scholten, I. Sinev, H. Mistry, B. Roldan Cuenya, *Angew. Chem. Int. Ed.*, 2018, **57**, 6192-6197.
- 17 X. Wang, A. Xu, F. Li, S.-F. Hung, D.-H. Nam, C. M. Gabardo, Z. Wang, Y. Xu, A. Ozden, A. S. Rasouli, A. H. Ip, D. Sinton, E. H. Sargent, *J. Am. Chem. Soc.*, 2020, **142**, 3525-3531.
- 18 E. L. Clark, J. Resasco, A. Landers, J. Lin, L.-T. Chung, A. Walton, C. Hahn, T. F. Jaramillo, A. T. Bell, *ACS Catal.*, 2018, **8**, 6560-6570.
- 19 R. Kortlever, J. Shen, K. J. P. Schouten, F. Calle-Vallejo, M. T. M. Koper, *J. Phys. Chem. Lett.*, 2015, **6**, 4073-4082.
- 20 S. Nitopi, E. Bertheussen, S. B. Scott, X. Liu, A. K. Engstfeld, S. Horch, B. Seger, I. E. L. Stephens, K. Chan, C. Hahn, J. K. Noerskov, T. F. Jaramillo, I. Chorkendorff, *Chem. Rev.*, 2019, **119**, 7610-7672.
- 21 F. Dattila, R. R. Seemakurthi, Y. Zhou, N. Lopez, *Chem. Rev.*, 2022, **122**, 11085-11130.
- 22 A. R. Woldu, Z. Huang, P. Zhao, L. Hu, D. Astruc, *Coord. Chem. Rev.*, 2021, **454**, 214340.
- 23 D. T. Whipple, P. J. A. Kenis, *J. Phys. Chem. Lett.*, 2010, **1**, 3451-3458.
- 24 K. C. Poon, W. Y. Wan, H. Su, H. Sato, *RSC Adv.*, 2022, **12**, 22703-22721.
- 25 S. Garg, M. Li, A. Z. Weber, L. Ge, L. Li, V. Rudolph, G. Wang, T. E. Rufford, *J. Mater. Chem. A*, 2020, **8**, 1511-1544.
- 26 M. S. Xie, B. Y. Xia, Y. Li, Y. Yan, Y. Yang, Q. Sun, S. H. Chan, A. Fisher, X. Wang, *Energy Environ. Sci.*, 2016, **9**, 1687-1695.
- 27 L. M. Aeshala, R. Uppaluri, A. Verma, *Phys. Chem. Chem. Phys.*, 2014, **16**, 17588-17594.
- 28 S. Ahn, K. Klyukin, R. J. Wakeham, J. A. Rudd, A. R. Lewis, S. Alexander, F. Carla, V. Alexandrov, E. Andreoli, *ACS Catal.*, 2018, **8**, 4132-4142.
- 29 S. Zhong, X. Yang, Z. Cao, X. Dong, S. M. Kozlov, L. Falivene, J.-K. Huang, X. Zhou, M. N. Hedhili, Z. Lai, K.-W. Huang, Y. Han, L. Cavallo, L.-J. Li, *ChemComm*, 2018, **54**, 11324-11327.
- 30 A. K. Buckley, M. Lee, T. Cheng, R. V. Kazantsev, D. M. Larson, W. A. I.I.I. Goddard, F. D. Toste, F. M. Toma, *J. Am. Chem. Soc.*, 2019, **141**, 7355-7364.
- 31 J. Wang, T. Cheng, A. Q. Fenwick, T. N. Baroud, A. Rosas-Hernandez, J. H. Ko, Q. Gan, W. A. I.I.I. Goddard, R. H. Grubbs, *J. Am. Chem. Soc.*, 2021, **143**, 2857-2865.
- 32 D. Wakerley, S. Lamaison, F. Ozanam, N. Menguy, D. Mercier, P. Marcus, M. Fontecave, V. Mougel, *Nat. Mater.*, 2019, **18**, 1222-1227.
- 33 F. P. Garcia de Arquer, C.-T. Dinh, A. Ozden, J. Wicks, C. McCallum, A. R. Kirmani, D.-H. Nam, C. Gabardo, A. Seifitokaldani, X. Wang, Y. C. Li, F. Li, J. Edwards, L. J. Richter, S. J. Thorpe, D. Sinton, E. H. Sargent, *Science*, 2020, **367**, 661-666.
- 34 C. Lu, Y. Su, J. Zhu, J. Sun, X. Zhuang, *ChemComm*, 2023, **59**, 6827-6836.
- 35 P. Chen, Y. Wu, T. E. Rufford, L. Wang, G. Wang, Z. Wang, *Mater. Today Chem.*, 2023, **27**, 101328.
- 36 C. V. Raman, K. S. Krishnan, *Nature*, 1928, **121**, 501-2.
- 37 M. Fleischmann, P. J. Hendra, A. J. McQuillan, *Chem. Phys. Lett.*, 1974, **26**, 163-6.
- 38 A. J. McQuillan, P. J. Hendra, M. Fleischmann, *J. Electroanal. Chem.*, 1975, **65**, 933-44.
- 39 M. G. Albrecht, J. A. Creighton, *J. Am. Chem. Soc.*, 1977, **99**, 5215-17.
- 40 Y. X. Chen, A. Miki, S. Ye, H. Sakai, M. Osawa, *J. Am. Chem. Soc.*, 3771, **125**, 3680-3681.
- 41 A. Miki, S. Ye, T. Senzaki, M. Osawa, *J. Electroanal. Chem.*, 2004, **563**, 23-31.
- 42 X. Chang, S. Vijay, Y. Zhao, N. J. Oliveira, K. Chan, B. Xu, *Nat. Commun.*, 2022, **13**, 2656.
- 43 D. L. Jeanmaire, R. P. Van Duyne, *J. Electroanal. Chem.*, 1977, **84**, 1-20.
- 44 I. V. Chernyshova, P. Somasundaran, S. Ponnurangam, *Proc. Natl. Acad. Sci. USA*, 2018, **115**, E9261-E9270.
- 45 I. Oda, H. Ogasawara, M. Ito, *Langmuir*, 1996, **12**, 1094-7.
- 46 H. Ogasawara, J. Inukai, M. Ito, *Chem. Phys. Lett.*, 1992, **198**, 389-94.
- 47 L. Mandal, K. R. Yang, M. R. Motapothula, D. Ren, P. Lobaccaro, A. Patra, M. Sherburne, V. S. Batista, B. S. Yeo, J. W. Ager, J. Martin, T. Venkatesan, *ACS Appl. Mater. Interfaces*, 2018, **10**, 8574-8584.
- 48 C. Zhan, F. Dattila, C. Rettenmaier, A. Bergmann, S. Kuehl, R. Garcia-Muelas, N. Lopez, B. R. Cuenya, *ACS Catal.*, 2021, **11**, 7694-7701.
- 49 T.-C. Chou, C.-C. Chang, H.-L. Yu, W.-Y. Yu, C.-L. Dong, J.-J. Velasco-Velez, C.-H. Chuang, L.-C. Chen, J.-F. Lee, J.-M. Chen, H.-L. Wu, *J. Am. Chem. Soc.*, 2020, **142**, 2857-2867.
- 50 Y. Wang, J. Zhang, J. Zhao, Y. Wei, S. Chen, H. Zhao, Y. Su, S. Ding, C. Xiao, *ACS Catal.*, 2024, **14**, 3457-3465.
- 51 C. M. Gunathunge, X. Li, J. Li, R. P. Hicks, V. J. Ovalle, M. M. Waegele, *J. Phys. Chem. C*, 2017, **121**, 12337-12344.
- 52 J. F. Li, Y. F. Huang, Y. Ding, Z. L. Yang, S. B. Li, X. S. Zhou, F. R. Fan, W. Zhang, Z. Y. Zhou, D. Y. Wu, B. Ren, Z. L. Wang, Z. Q. Tian, *Nature*, 2010, **464**, 392-395.
- 53 Y. Zhao, X. Chang, A. S. Malkani, X. Yang, L. Thompson, F. Jiao, B. Xu, *J. Am. Chem. Soc.*, 2020, **142**, 9735-9743.
- 54 Y. Zhao, X.-G. Zhang, N. Bodappa, W.-M. Yang, Q. Liang, P. M. Radjenovica, Y.-H. Wang, Y.-J. Zhang, J.-C. Dong, Z.-Q. Tian, J.-F. Li, *Energy Environ. Sci.*, 2022, **15**, 3968-3977.
- 55 V. J. Ovalle, M. M. Waegele, *J. Phys. Chem. C*, 2019, **123**, 24453-24460.
- 56 Z. Han, R. Kortlever, H.-Y. Chen, J. C. Peters, T. Agapie, *ACS Cent. Sci.*, 2017, **3**, 853-859.
- 57 Z. Liu, X. Lv, S. Kong, M. Liu, K. Liu, J. Zhang, B. Wu, Q. Zhang, Y. Tang, L. Qian, L. Zhang, G. Zheng, *Angew. Chem. Int. Ed.*, 2023, **62**, e202309319.
- 58 L. Xue, X. Wu, Y. Liu, B. Xu, X. Wang, S. Dai, P. Liu, H. Yang, *Nano Res.*, 2022, **15**, 1393-1398.
- 59 J. R. Pankhurst, P. Iyengar, A. Loiudice, M. Mensi, R. Buonsanti, *Chem. Sci.*, 2020, **11**, 9296-9302.
- 60 G.-R. Zhang, S.-D. Straub, L.-L. Shen, Y. Hermans, P. Schmatz, A. M. Reichert, J. P. Hofmann, I. Katsounaros, B. J. M. Etzold, *Angew. Chem. Int. Ed.*, 2020, **59**, 18095-18102.



- 61 J. Li, F. Li, C. Liu, F. Wei, J. Gong, W. Li, L. Xue, J. Yin, L. Xiao, G. Wang, J. Lu, L. Zhuang, *ACS Energy Lett.*, 2022, **7**, 4045-4051.
- 62 C. Y. J. Lim, M. Yilmaz, J. M. Arce-Ramos, A. D. Handoko, W. J. Teh, Y. Zheng, Z. H. J. Khoo, M. Lin, M. Isaacs, T. L. D. Tam, Y. Bai, C. K. Ng, B. S. Yeo, G. Sankar, I. P. Parkin, K. Hippalgaonkar, M. B. Sullivan, J. Zhang, Y.-F. Lim, *Nat. Commun.*, 2023, **14**, 335.
- 63 C. E. Creissen, J. G. Rivera de la Cruz, D. Karapinar, D. Taverna, M. W. Schreiber, M. Fontecave, *Angew. Chem. Int. Ed.*, 2022, **61**, e202206279.
- 64 J. Ding, F. Li, X. Ren, Y. Liu, Y. Li, Z. Shen, T. Wang, W. Wang, Y.-G. Wang, Y. Cui, H. Yang, T. Zhang, B. Liu, *Nat. Commun.*, 2024, **15**, 3641.
- 65 Y. Wang, R. Zhao, Y. Liu, F. Zhang, Y. Wang, Z. Wu, B. Han, Z. Liu, *Chem. Sci.*, 2024, **15**, 4140-4145.
- 66 F. Li, A. Thevenon, A. Rosas-Hernandez, Z. Wang, Y. Li, C. M. Gabardo, A. Ozden, C. T. Dinh, J. Li, Y. Wang, J. P. Edwards, Y. Xu, C. McCallum, L. Tao, Z.-Q. Liang, M. Luo, X. Wang, H. Li, C. P. O'Brien, C.-S. Tan, D.-H. Nam, R. Quintero-Bermudez, T.-T. Zhuang, Y. C. Li, Z. Han, R. D. Britt, D. Sinton, T. Agapie, J. C. Peters, E. H. Sargent, *Nature*, 2020, **577**, 509-513.
- 67 Y. Shi, K. Sun, J. Shan, H. Li, J. Gao, Z. Chen, C. Sun, Y. Shuai, Z. Wang, *ACS Catal.*, 2022, **12**, 8252-8258.
- 68 S. Mu, L. Li, R. Zhao, H. Lu, H. Dong, C. Cui, *ACS Appl. Mater. Interfaces*, 2021, **13**, 47619-47628.
- 69 L. Huang, G. Gao, C. Yang, X.-Y. Li, R. K. Miao, Y. Xue, K. Xie, P. Ou, C. T. Yavuz, Y. Han, G. Magnotti, D. Sinton, E. H. Sargent, X. Lu, *Nat. Commun.*, 2023, **14**, 2958.
- 70 S. Banerjee, Z.-Q. Zhang, A. S. Hall, V. S. Thoi, *ACS Catal.*, 2020, **10**, 9907-9914.
- 71 J. Resasco, L. D. Chen, E. Clark, C. Tsai, C. Hahn, T. F. Jaramillo, K. Chan, A. T. Bell, *J. Am. Chem. Soc.*, 2017, **139**, 11277-11287.
- 72 X. Yang, H. Ding, S. Li, S. Zheng, J.-F. Li, F. Pan, *J. Am. Chem. Soc.*, 2024, **146**, 5532-5542.
- 73 Z. Tao, Z. Wu, Y. Wu, H. Wang, *ACS Catal.*, 2020, **10**, 9271-9275.
- 74 A. T. Chu, Y. Surendranath, *J. Am. Chem. Soc.*, 2022, **144**, 5359-5365.
- 75 X. Bai, C. Chen, X. Zhao, Y. Zhang, Y. Zheng, Y. Jiao, *Angew. Chem. Int. Ed.*, 2024, **63**, e202317512.
- 76 Y. Lin, T. Wang, L. Zhang, G. Zhang, L. Li, Q. Chang, Z. Pang, H. Gao, K. Huang, P. Zhang, Z.-J. Zhao, C. Pei, J. Gong, *Nat. Commun.*, 2023, **14**, 3575.
- 77 T. H. M. Pham, J. Zhang, M. Li, T.-H. Shen, Y. Ko, V. Tileli, W. Luo, A. Zuttel, *Adv. Energy Mater.*, 2022, **12**, 2103663.
- 78 X. Wei, Z. Yin, K. Lyu, Z. Li, J. Gong, G. Wang, L. Xiao, J. Lu, L. Zhuang, *ACS Catal.*, 2020, **10**, 4103-4111.
- 79 S. Zhao, O. Christensen, Z. Sun, H. Liang, A. Bagger, K. Torbensen, P. Nazari, J. V. Lauritsen, S. U. Pedersen, L. Rossmeyl, K. Daasbjerg, *Nat. Commun.*, 2023, **14**, 844.
- 80 Y. Zhao, X. Zu, R. Chen, X. Li, Y. Jiang, Z. Wang, S. Wang, Y. Wu, Y. Sun, Y. Xie, *J. Am. Chem. Soc.*, 2022, **144**, 10446-10454.
- 81 H.-Q. Liang, S. Zhao, X.-M. Hu, M. Ceccato, T. Skrydstrup, K. Daasbjerg, *ACS Catal.*, 2021, **11**, 958-966.
- 82 B. Zhao, F. Chen, C. Cheng, L. Li, C. Liu, B. Zhang, *Adv. Energy Mater.*, 2023, **13**, 2204346.
- 83 K. N. Kolding, M. Bretlau, S. Zhao, M. Ceccato, K. Torbensen, K. Daasbjerg, A. Rosas-Hernandez, *J. Am. Chem. Soc.*, 2024, **146**, 13034-13045.
- 84 Y. Yao, T. Shi, W. Chen, J. Wu, Y. Fan, Y. Liu, L. Cao, Z. Chen, *Nat. Commun.*, 2024, **15**, 1257.
- 85 N. B. Watkins, Y. Wu, W. Nie, J. C. Peters, T. Agapie, *ACS Energy Lett.*, 2023, **8**, 189-195.
- 86 A. Thevenon, A. Rosas-Hernandez, J. C. Peters, T. Agapie, *Angew. Chem. Int. Ed.*, 2019, **58**, 16952-16958.
- 87 T. Kim, G. T. R. Palmore, *Nat. Commun.*, 2020, **11**, 3622.
- 88 R. Reske, H. Mistry, F. Behafarid, B. Roldan Cuenya, P. Strasser, *J. Am. Chem. Soc.*, 2014, **136**, 6978-6986.
- 89 K. Manthiram, B. J. Beberwyck, A. P. Alivisatos, *J. Am. Chem. Soc.*, 2014, **136**, 13319-13325. [DOI: 10.1039/D4CC03973D](https://doi.org/10.1039/D4CC03973D)
- 90 A. Loiudice, P. Lobaccaro, E. A. Kamali, T. Thao, B. H. Huang, J. W. Ager, R. Buonsanti, *Angew. Chem. Int. Ed.*, 2016, **55**, 5789-5792.
- 91 W. Rong, H. Zou, W. Zang, S. Xi, S. Wei, B. Long, J. Hu, Y. Ji, L. Duan, *Angew. Chem. Int. Ed.*, 2021, **60**, 466-472.
- 92 R. Igarashi, R. Takeuchi, K. Kubo, T. Mizuta, S. Kume, *Front. Chem.*, 2019, **7**, 860.
- 93 R. Takeuchi, R. Igarashi, K. Kubo, T. Mizuta, S. Kume, *ChemElectroChem*, 2020, **7**, 2575-2581.
- 94 T. Umeda, T. Kurome, A. Sakamoto, K. Kubo, T. Mizuta, S. U. Son, S. Kume, *ChemComm*, 2022, **58**, 8053-8056.



Data Availability Statement

Title: Spectrometric Monitoring of CO₂ Electrolysis on a Molecularly Modified Copper Surface

Akiyoshi Kuzume* and Shoko Kume*

No primary research results, software or code have been included and no new data were generated or analysed as part of this review.

